9-2010

Phase diagram of unpoled lead-free (1-x)(Bi1/2Na1/2)TiO3–xBaTiO3 ceramics

C. Ma
Iowa State University

Xiaoli Tan
Iowa State University, xtan@iastate.edu

Phase diagram of unpoled lead-free (1-x)(Bi1/2Na1/2)TiO3–xBaTiO3 ceramics

Abstract
A phase diagram for unpoled ceramics in the lead-free (1–x)(Bi1/2Na1/2)TiO3–xBaTiO3 binary system is constructed for the first time based on transmission electron microscopy (TEM) and dielectric study. In contrast to the reported phase diagram determined using poled ceramics, an additional phase region exhibiting *P4bm* nanodomains was revealed. A new concept "relaxor antiferroelectric" was proposed to describe the unique short-range antiferroelectric order of this phase. The results suggest that electric field-induced phase transitions must be taken into consideration in optimizing the piezoelectric properties in these lead-free ceramics.

Keywords
Lead-free piezoelectrics, domain structure, phase diagram, transmission electron microscopy

Disciplines
Ceramic Materials | Metallurgy

Phase diagram of unpoled lead-free (1-*x*)($Bi_{1/2}Na_{1/2}$)TiO_3–*x*$BaTiO_3$ ceramics

C. Ma and X. Tan[a)]

Department of Materials Science and Engineering, Iowa State University, Ames, IA 50014 USA

a)Electronic mail: xtan@iastate.edu

ABSTRACT

A phase diagram for unpoled ceramics in the lead-free (1-*x*)($Bi_{1/2}Na_{1/2}$)TiO_3–*x*$BaTiO_3$ binary system is constructed for the first time based on transmission electron microscopy (TEM) and dielectric study. In contrast to the reported phase diagram determined using poled ceramics, an additional phase region exhibiting *P4bm* nanodomains was revealed. A new concept "relaxor antiferroelectric" was proposed to describe the unique short-range antiferroelectric order of this phase. The results suggest that electric field-induced phase transitions must be taken into consideration in optimizing the piezoelectric properties in these lead-free ceramics.

Keywords: Lead-free piezoelectrics, domain structure, phase diagram, transmission electron microscopy

For the past five decades, lead-containing perovskite ceramics based on solid solution $Pb(Zr_{1-x}Ti_x)O_3$ (PZT) have been dominating the markets of piezoelectric transducers and actuators due to their excellent piezoelectric performance, ease of processing, and low cost [1]. However, the toxicity of lead has raised serious environmental concerns and the restriction of lead use in electronic devices is now demanded by legislations in the European Union and part of Asia [2]. This makes the search for lead-free replacement for PZT an urgent task. The $(Bi_{1/2}Na_{1/2})TiO_3$-$BaTiO_3$ (BNT-BT) solid solution has long been regarded as one of the most promising candidates for piezoelectric applications [2-5]. Piezoelectric properties were observed to peak at the morphotropic phase boundary (MPB) at $x \approx 0.06$ in the (1-*x*)BNT-*x*BT system [3, 5].

Although much progress has been made in literature on the (1-*x*)BNT-*x*BT binary system, including the proposed and refined phase diagrams around the MPB [3, 4], there are still fundamental issues that need to be clarfied. First of all, these phase diagrams are obtained from poled ceramics. One of the critical temperatures, T_d, does not even exist in certain compositions in the unpoled state [6]. A recent X-ray diffraction study indicated that a pseudocubic-to-tetragonal phase transition occurs during the poling process and the induced tetragonal phase persists when the applied field is removed [7]. Obviously the phase diagram for unpoled (1-*x*)BNT-*x*BT ceramics is different from that of poled ceramics. However, the phase diagram for unpoled ceramics has not yet been reported in literatrue. Secondly, only a limited number of studies on ferroelectric domain structures in (1-*x*)BNT-*x*BT ceramics were reported, and most of them are inconsistent [8-10]. In the single crystals of 0.97BNT-0.03BT and 0.92BNT-0.08BT, it was claimed that no signs of ferroelectric domains exist [8]. Recently nanodomains of tilted oxygen octahedra were imaged using the dark field technique in transmission electron microscopy (TEM) in the 0.90BNT-0.05BT-0.05$(Bi_{1/2}K_{1/2})TiO_3$ ceramic [9], but large lamellar

ferroelectric domains in the ceramic 0.94BNT–0.05BT–0.01($K_{0.5}Na_{0.5}$)NbO_3 were also observed [10]. Ferroelectric domains are known to be the fundamental microstructural units dictating the dielectric, ferroelectric and piezoelectric properties of these functional ceramics. However, it is very difficult to obtain a full picture on the correlation of domain morphology with chemical composition in (1-*x*)BNT-*x*BT ceramics from these individual reports.

The phase diagram of unpoled (1-*x*)BNT-*x*BT ceramics is an indispensable tool to guiding the search for compositions with optimum properties and understanding the origin of electric-field-induced strain in this system. In this communication, this phase diagram is constructed for the first time based on the results from dielectric characterization and TEM examination of domain morphologies in a series of compositions in (1-*x*)BNT-*x*BT in the unpoled state. Compared with the phase diagram for poled ceramics, siginiciant differences are noticed. For example, an additional phase region exhibiting *P4bm* symmetry and unique relaxor characteristics was revealed in the composition range $0.07 \leq x \leq 0.09$ at room temperature

Polycrystalline ceramic samples of (1-*x*)BNT-*x*BT (x = 0.04, 0.06, 0.07, 0.09, 0.11) were prepared via the solid state reaction approach. Stoichiometric amount of reagent grade powders of Bi_2O_3 (≥99.9%), Na_2CO_3 (≥99.9 %), $BaCO_3$ (≥99.99%) and TiO_2 (≥99.99%) were mixed and vibratory milled in ethanol with zirconia mill media for 7 hours and then dried. The Na_2CO_3 powder was baked at 200 °C for 15 hours and then weighed immediately to ensure the stoichiometry. The mixture was calcined at 800 ºC for 2 hours and then vibratory milled for another 16 hours. After drying, the powders were evenly mixed with the binder (10 wt% polyvinyl alcohol solution) and then uniaxially pressed into pellets. Following the binder burnout at 500 ºC, sintering was carried out at 1150 ºC for 5 hours. In order to prevent the loss of Bi^{3+} and Na^+, the pellets were buried in a plenty amount of protective powder with the same

composition during sintering. The relative density of the sintered pellets are higher than 95% as determined by the Archimedes' method. Scanning electron microscopy observations indicate that the grain size slightly decreases with increasing x. The average grain size is ~3 μm for the composition with $x = 0.04$, and ~2 μm for that with $x = 0.11$. X-ray diffraction experiments were performed on as-sintered ceramic surfaces with a PANalytical X'pert PRO MPD X-ray diffractometer with monochromatic CuKα radiation in the step scanning mode with increments of 0.05º. Pure perovskite phases were confirmed in all the samples.

The surfaces of as-sintered ceramic pellets were polished and made parallel prior to electrical measurements. Fired on silver paste (Dupont 6160) was then applied as electrodes. Dielectric constant and loss tangent under weak electric field was measured with an LCR meter (HP-4284A, Hewlett-Packard) in conjugation with a tube furnace during heating at a rate of 3 °C/min. TEM specimens were prepared from the as-sintered pellets through standard procedures including grinding, cutting, dimpling and ion milling. The dimpled disks were annealed at 250 ºC for 2 hours to minimize the residual stresses before Ar-ion mill to electron transparency. TEM studies were carried out on a Phillips CM-30 microscope operated at 300 kV.

The compositions studied can be grouped into three categories according to their dielectric behaviors in the unpoled state: $x \leq 0.06$, $0.07 \leq x \leq 0.09$, and $x \geq 0.11$. The temperature dependence of the relative dielectric permittivity ε_r and loss tangent $\tan\delta$ for the representatvie compositions of these three groups were plotted in Fig. 1. The features of the curves and their variation with the composition are consistent with previous studies [3]. For the compositions $x \leq 0.06$ (as represented by $x = 0.06$) and $x \geq 0.11$ (as represented by $x = 0.11$), a sharp increase of ε_r was observed at T_d, which has been denoted as the ferroelectric-antiferroelectric transition temperature in literature [4]. The frequency dispersion in ε_r and $\tan\delta$ is minimum at temperatures

below T_d but suddenly becomes significant above T_d. With further increase in temperature, the frequency dispersion vanishes before reaching T_m, the temperature where ε_r reaches a maximum. We define an additional critical temperature, T_{RE}, to mark the temperature where the frequency dispersion vanishes. While the minimum frequency dispersion below T_d and the sharp anomaly at T_d characterize the long-range ferroelectric order, the strong frequency dispersion in ε_r and tanδ between T_d and T_{RE} seems to suggest the phase that was previously believed as antiferroelectric in this temperature window has relaxor characteristics [3, 10].

In contrast to the two composition regions discussed above, for $0.07 \leq x \leq 0.09$ (as represented by $x = 0.07$), no sharp anomaly exists in either the ε_r *vs.* T or the tanδ *vs.* T curve to locate T_d. The frequency dispersion in ε_r and tanδ is significant even at room temperature and persists up to T_{RE}. The absence of T_d and the significant frequency dispersion from room temperature up to T_{RE} indicate the high-temperature antiferroelectric phase with relaxor characteristics persists down to room temperature in the unpoled state for compositions $0.07 \leq x \leq 0.09$. Note that the relaxor characteristics associated with the antiferroelectric phase is different from the classical relaxor ferroelectrics: T_{RE} does not coincide with T_m as the prototype relaxor $Pb(Mg_{1/3}Nb_{2/3})O_3$ does [11]. The results of the dielectric characterization clearly indicate that at room temperature the unpoled (1-*x*)BNT-*x*BT ceramics display long range ferroelectric order for $x \leq 0.06$ and $x \geq 0.11$, while exhibit relaxor behaviors for $0.07 \leq x \leq 0.09$.

Excellent correlations of the room temperature dielectric behavior with the domain structure were found in unpoled (1-*x*)BNT-*x*BT ceramics. For $x \leq 0.06$, ferroelectric domains around ~100 nm in size with well-defined domain walls were observed by TEM bright field imaging. These ferroelectric domains form complex patterns and dominate all the grains in the ceramic of $x = 0.04$. As x increases to 0.06, mixed phases in many grains were observed: the ferroelectric

domains (~100 nm in size) reside in a volume within the grains, and nanodomains are found in the region surrounding these volumes. Around 40 % of the grains in $x = 0.06$ display such mixed-phase grain structure, while the rest exhibit nanodomains only. Figure 2 shows a representative grain for $x = 0.06$ imaged along its [011] and [111] zone axes, respectively (The miller indices in this communication are based on the parent cubic cell of the simple perovskite structure). The volume within the grain with the ~100 nm sized ferroelectric domains is marked by the brigh arrow in Fig. 2(a) and 2(d). When tilted to the [011] zone axis, some domain walls of the ~100 nm ferroelectric domains are at the edge-on position and were determined to be the {100} planes. When tilted to the [111] zone axis, these domain walls are inclined with respect to the electron beam direction and no sharp domain walls can be oberved. This domain morphology does not resemble any of the previously reported one including pure $(Bi_{1/2}Na_{1/2})TiO_3$ [12]. We refer to this morphology of 100nm-sized domains as "complex domains". The morphology of the nanodomains (< 20 nm) in the surrounding region of the grain does not exhibit noticeable difference when imaged along the [011] and the [111] zone axes.

The crystal structure of these two types of domains can be determined by the selected area electron diffraction (SAED). According to previous studies [3, 4], only perovskite phases with *R3c*, *P4mm* and *P4bm* symmetries need to be considered for (1-*x*)BNT-*x*BT ceramics at room temperature. Electron diffraction analysis indicates that the complex domains in the interior volume of the grain exhibit the *R3c* symmetry as evidenced by the presence of strong $\frac{1}{2}(ooo)$ (*o* denotes odd Miller indices) superlattice spots along the [011] zone axis and the absence of any superlattice spots along the [111] zone axis [13, 14]. This is isostructural to $(Bi_{1/2}Na_{1/2})TiO_3$ at room temperature with the $a^-a^-a^-$ oxygen octahedron tilt [14, 15]. In contrast, the surrounding region with nanodomains was determined to be isostructural with the high-temperature

antiferroelectric phase of $(Bi_{1/2}Na_{1/2})TiO_3$ exhibiting *P4bm* symmetry with the $a^0a^0c^+$ oxygen octahedron tilt [15], as evidenced by the presence of strong $\frac{1}{2}(ooe)$ (*e* denotes even Miller indices) superlattice diffraction sptots along the [111] zone axis and the absence of any superlattice spots along the [011] zone axis [12, 13]. Furthermore, the presence of all the variants of the $\frac{1}{2}(ooe)$ superlattice spots in Fig. 2(e) indicates that the surrounding region contains all the variants of antiferroelectric domains. The coexistence of the *R3c* complex domains and *P4bm* nanodomains indicates a composition-induced phase transition occuring at $x = 0.06$. The presence of *R3c* complex domains for $x \leq 0.06$ is consistent with the long-range ferroelectric order observed below T_d [Fig. 1(a)].

With increasing x to 0.07 and 0.09, only nanodomains with *P4bm* symmetry were observed in all grains at room temperature. The morphology of the nanodomains in these two compositions is nearly the same as those in $x = 0.06$. The presence of only *P4bm* nanodomains at room temperature in compositions $0.07 \leq x \leq 0.09$ appears to correlate well with the absence of T_d and the persistance of the high-temperature antiferroelectric phase with relaxor characteristics down to room temperature in these compositions [Fig. 1(b)]. There has been a debate about the nature of this *P4bm* phase in (1-*x*)BNT-*x*BT ceramics: the pinched polarization hysteresis loop suggests an antiferroelectric behavior [3], while the absence of large domains and the almost linear elastic deformation seem to indicate a relaxor behavior [10]. Based on our TEM results, we propose a concept "relaxor antiferroelectric" to reconcile this discrepancy. We speculate that these nanodomains exhibit antiferroelectric ordering within them, as supported by the presence of antiparallel cation displacements in the crystal structure of the *P4bm* phase in $(Bi_{1/2}Na_{1/2})TiO_3$ [15]. In the meanwhile, similar to the relaxor ferroelectric [16], the randomly

oriented and dynamically fluctuating antiparallel dipoles in these nanodomains give rise to relaxor characteristics like frequency dispersion and diffused transition. The existence of randomly oriented antiferroelectric nanodomains is supported by the presence of all the variants of the $\frac{1}{2}(ooe)$ superlattice spots in Fig. 2(e). Such relaxor antiferroelectric behavior persists from room temperature up to T_{RE} in $0.07 \leq x \leq 0.09$, and would dominate in the compositions $x \leq 0.06$ and $x \geq 0.11$ between T_d and T_{RE}.

For the composition $x = 0.11$, large lamellar ferroelectric domains prevail (not shown). Around 20% of the grains exhibit both *P4bm* nanodomains and lamellar domains, and the rest display lamellar domains only. Electron diffraction analysis indicates that the lamellar domains have {101} domain walls. No superlattice spot was observed along either [011] or [111] zone axis from volume with large lamellar domains, indicating no oxygen octahedron tilt is present. These are precisely the characteristic domain features of the *P4mm* $BaTiO_3$ [17]. The mixed phases in $x = 0.11$ suggest a phase transition from *P4bm* to *P4mm* occuring. The dominating amount of the large lamellar ferroelectric domains with long range ferroelectric order explains the minimum frequency dispersion in the dielectric behavior [Fig. 1(c)].

It should be noted that the mixed phases observed by TEM in $x = 0.06$ and 0.11 could be a result of chemical inhomogeneity within individual grains. However, the extended sintering time (5 hours at 1150 ºC) is expected to minimize such composition variation. This is supported by the TEM observation on ceramics of $x = 0.04$, 0.07, and 0.09 where uniform microstructure is seen. Therefore, it is highly likely that the mixed phases in $x = 0.06$ and 0.11 are due to mechanical as well as electrical conditions at grain boundaries. It should also be noted that such mechanical and electrical conditions could be different in TEM thin specimens from that in bulk samples. Particularly, this difference may lead to a higher volume fraction of the *R3c* complex

domains in bulk samples of the ceramic $x = 0.06$ on which the prominent transition at T_d was revealed by the dielectric characterization [Fig. 1(a)].

Combining the results from the macroscopic dielectric characterization and those from the nanoscale domain morphology and crystal structure analysis with TEM, a phase diagram for unpoled (1-*x*)BNT-*x*BT ceramics can be constructed (Fig. 3). The room-temperature crystal structure and domain morphology are highlighted as shaded boxes. Compared with the phase diagrams in literature for poled ceramics [3, 4], the difference is significant. First of all, an additional phase region exhibiting *P4bm* symmetry was revealed between the ferroelectric *R3c* and *P4mm* phase regions at room temperature. The $x = 0.06$ MPB separating *R3c* and *P4mm* ferroelectric phases in poled ceramics corresponds to a phase boundary between the ferroelectric *R3c* phase and the relaxor antiferroelectric *P4bm* phase in unpoled ceramics. Secondly, our phase diagram has accounted for the domain morphology and crystal structure, and excellent struture-property correlations were observed. For $x \leq 0.06$ and $x \geq 0.11$, the ferroelectric domains (> 100 nm) with well-defined domain walls were observed along with the long-range ferroelectric order at room temperature and are expected to persist up to T_d. For $0.07 \leq x \leq 0.09$, the room-temperature antiferroelectric nanodomains with irregular domain walls leading to the relaxor antiferroelectric behavior are expected to dominate up to T_{RE}. Such nanodomains with *P4bm* symmetry are also speculated to be the primary feature between T_d and T_{RE} in compositions $x \leq 0.06$ and $x \geq 0.11$. Thirdly, an additional critical temperature T_{RE} is identified and marked on the phase diagram. These results suggest that (1-*x*)BNT-*x*BT solid solution is a unique lead-free piezoelectric system: maximum piezoelectric properties were obtained at an MPB separating a ferroelectric and a relaxor antiferroelectric phase, instead of one separating two ferroelectric phases as in PZT [1]. The origin of the electric-field-induced strain in (1-

x)BNT-*x*BT around MPB may not be completely due to the piezoelectric nature. Two types of electric-field-induced phase transitions, i.e. the relaxor-to-ferroelectric and the antiferroelectric-to-ferroelectric, must be considered and investigated. In addition to the X-ray diffraction study [7], *in situ* TEM studies with applied electric fields are thus necessary to visualize the domain morphology evolution during these phase transitions [18, 19].

Acknowledgements

This work was supported by the National Science Foundation (NSF) through Grant DMR-1037898.

References

[1] B. Jaffe, W.R. Cook, H. Jaffe, Piezoelectric Ceramics, Academic Press, London, 1971.

[2] J. Rödel, W. Jo, K. Seifert, E.M. Anton, T. Granzow, D. Damjanovic, J. Am. Ceram. Soc. 92 (2009) 1153.

[3] T. Takenaka, K. Maruyama, K. Sakata, Jpn. J. Appl. Phys. Part 1 30 (1991) 2236.

[4] Y. Hiruma, Y. Watanabe, H. Nagata, T. Takenaka, Key Eng. Mater. 350 (2007) 93.

[5] C. Xu, D. Lin, K.W. Kwok, Solid State Sci. 10 (2008) 934.

[6] Y. Hiruma, H. Nagata, T. Takenaka, J. Appl. Phys. 104 (2008) 124106.

[7] J.E. Daniels, W. Jo, J. Rödel, J.L. Jones, Appl. Phys. Lett. 95 (2009) 032904.

[8] A.N. Soukhojak, H. Wang, G.W. Farrey, Y.M. Chiang, J. Phys. Chem. Solids 61 (2000) 301.

[9] C.W. Tai, Y. Lereah, Appl. Phys. Lett. 95 (2009) 062901.

[10] X. Tan, E. Aulbach, W. Jo, T. Granzow, J. Kling, M. Marsilius, H.J. Kleebe, J. Rödel, J. Appl. Phys. 106 (2009) 044107.

[11] X. Zhao, W. Qu, X. Tan, A.A. Bokov, Z.G. Ye, Phys. Rev. B 79 (2009) 144101.

[12] V. Dorcet, G. Trolliard, Acta Mater. 56 (2008) 1753.

[13] D.I. Woodward, I.M. Reaney, Acta Cryst. B61 (2005) 387.

[14] A.M. Glazer, Acta Cryst. A31 (1975) 756.

[15] G.O. Jones, P.A. Thomas, Acta Cryst. B58 (2002) 168.

[16] L.E. Cross, Ferroelectrics 76 (1987) 241.

[17] H. Hu, H.M. Chan, X.W. Zhang, M.P. Harmer, J. Am. Ceram. Soc. 69 (1986) 594.

[18] H. He, X. Tan, Phys. Rev. B 72 (2005) 024102.

[19] W. Qu, X. Zhao, X. Tan, J. Appl. Phys. 102 (2007) 084101.

Fig. 1. Temperature dependence of the dielectric constant ε_r and loss $tan\delta$ for x = 0.06, 0.07, and 0.11 measured during heating at 3 °C/min.

Fig. 2. (a) TEM bright field image of a typical grain with the mixed-phase structure for the composition x = 0.06 along its [011] zone axis. The volume with complex domains is marked by the bright arrow. (b) Diffraction pattern of nanodomains along [011] zone axis; (c) diffraction pattern of the complex domains along [011] zone axis; (d) TEM bright field image of the same grain tilted to its [111] zone axis; (e) diffraction pattern of nanodomains along [111] zone axis; (f) diffraction pattern of complex domains along [111] zone axis.

Fig. 3. The phase diagram for unpoled ceramics in the (1-x)BNT-xBT binary system. The solid triangles represent T_d, open circles for T_{RE}, and solid squares for T_m. FE stands for ferroelectric, AFE for antiferroelectric, and PE for paraelectric.

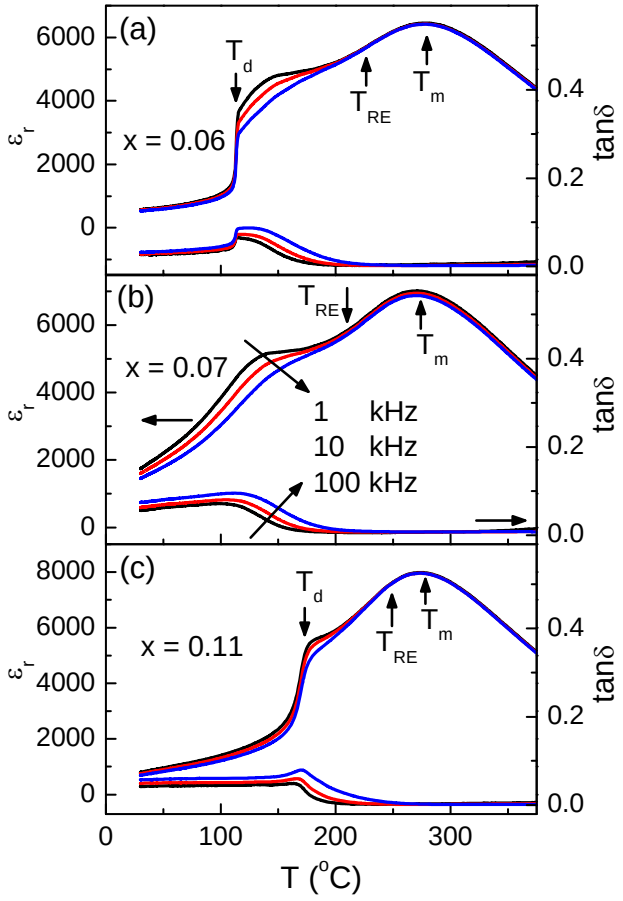
(a)
x = 0.06
T_d
T_RE
T_m
(b)
x = 0.07
T_RE
T_m
1 kHz
10 kHz
100 kHz
(c)
x = 0.11
T_d
T_RE
T_m
ε_r
tanδ
T (°C)

Fig. 1

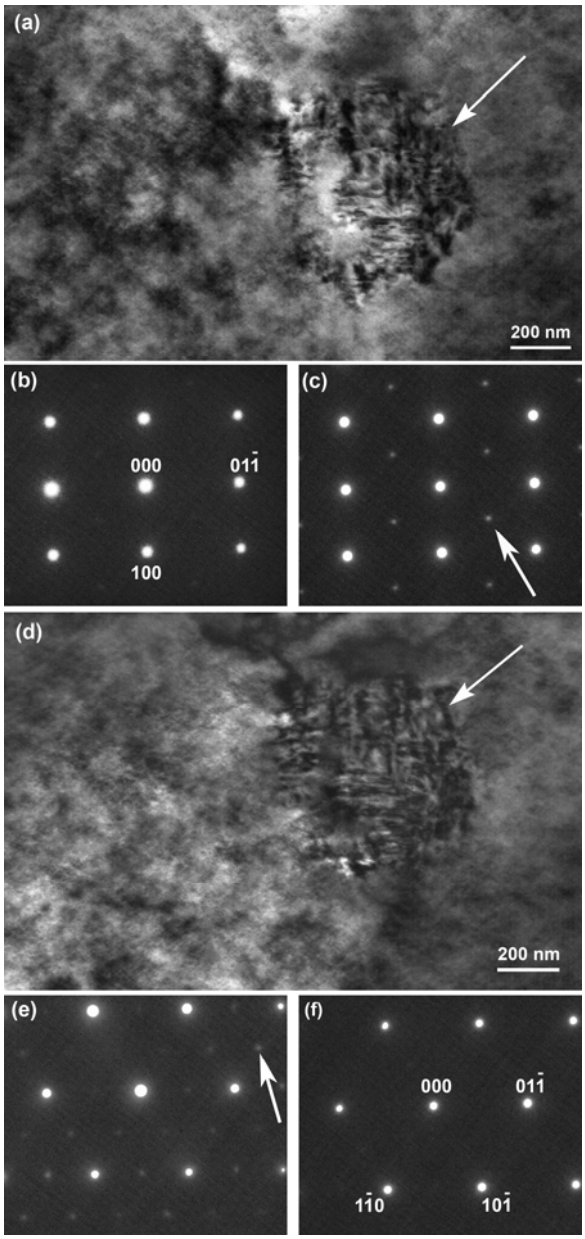

Fig. 2

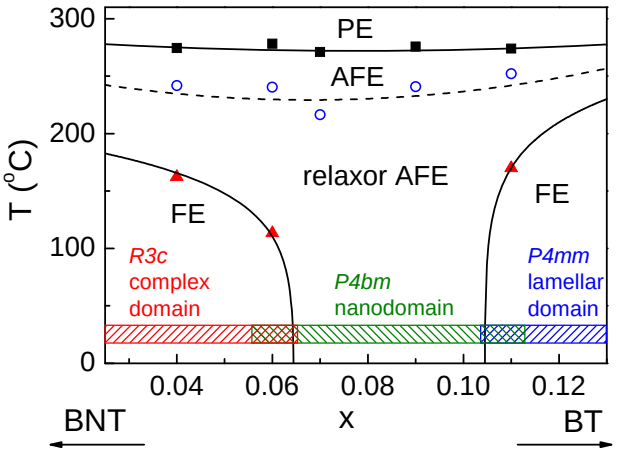
300
200
100
0
T (°C)
PE
AFE
relaxor AFE
FE
FE
R3c
complex
domain
P4bm
nanodomain
P4mm
lamellar
domain
0.04
0.06
0.08
0.10
0.12
x
BNT
BT

Fig. 3